https://doi.org/10.46813/2024-153-103

ELECTROPHYSICAL CHARACTERISTICS OF TiO_2 SAMPLES IRRADIATED WITH 0.12 MeV HELIUM IONS

K.V. Pavlii, S.N. Dubniuk, O.F. Dyachenko, O.V. Manuilenko, B.V. Zajtsev*
National Science Center "Kharkiv Institute of Physics and Technology", Kharkiv, Ukraine
**E-mail: kvint@kipt.kharkov.ua*

The main parameters of samples irradiation on the linear helium ions accelerator are presented as well as of TiO_2 irradiated characteristics. It is experimentally shown that with irradiation dose increasing, helium ion energy of 0.12 MeV, the volume electrical resistance and surface electrical resistances on the front and back sides of samples decrease, the loss angle tangents and relative dielectric permittivities increase. The primary processes, namely: the sputtering, ionization, phonons and vacancies formation, segregation, damage have been calculated. The analysis of experimental and calculated data has shown that a model based on processes of the excitation and propagation of elastic waves in a concept of the long-range effect most physically correctly describes the changes in electrophysical characteristics of the irradiated samples.

PACS: 62.20.Dc; 62.20.Fe

INTRODUCTION

The long-range effect is manifested in the anomalously deep propagation of defects induced by the ion irradiation [1, 2], in the dislocation structures formation, in the change of the structural-phase state, in the segregation of the main materials components in layers with a depth much greater than the run value [3, 4] and in the appearance of the implanted element on both sides of a target [1, 2]. Experimental results of this effect are shown in the microhardness change, wear resistance, etc. of metals [5–8], in the change of the resistivity, Hall constant, etc. of semiconductors and dielectrics [2, 9].

A number of models [3, 4, 10–13] and others have been created to theoretically describe of the long-range effect. A model based on the elastic wave excitation processes [4, 12, 13] most physically correctly describes some of the long-range effects. According to this model, a high-frequency acoustic wave appears in the irradiated material. This wave is converted either into a shock wave or propagates as an acoustic wave. Propagating through the sample volume, it causes defect rearrangement and secondary waves emission. The main factor for the remodeling processes is the shock wave pressure. However, due to the multitude of the long-range effects, there is no single mechanism to explain this phenomenon.

The purpose of this work is to confirm of the long-range effects by obtaining of the experimental results (electrophysical characteristics) after irradiation of TiO_2-based samples, calculation of the primary processes occurring in the course of the irradiation, and analyzing of the obtained experimental and calculated data.

1. IRRADIATION PARAMETERS AND SAMPLE CHARACTERISTICS

In NSC KIPT the linear helium ions (He^+) accelerator works [14–16]. The basic parameters of helium ions beam at an irradiation of samples on the linear accelerator are resulted in Table 1. The papers [15–18] present experimental methods and some investigation results of the microscopic, electrophysical and frictional characteristics of the structural materials obtained on the linear accelerator of helium ions with 0.12 and 4 MeV energies. The irradiation parameters were recorded using digital devices that are connected to a computer for further processing [19].

The irradiation of TiO_2-1 and TiO_2-2 samples was carried out at 120 keV, which is the injector energy [14, 15]. The injector main parameters are given in Table 2.

Table 1
Irradiation parameters

Parameter	Value
Beam energy, MeV	0.12…4
Pulse current, μA	1100…300
Pulse length, μs	500
Current density, part./cm^2	$(0.44…0.15)\cdot10^{13}$
Repetition rate, imp./s	2…5

Table 2
Injector main parameters

Working gas	helium
Arc current, A	2…4
Output beam current, mA	up to 20
Particle energy at the output, keV	120
Output beam diameter, mm	~ 10
Working gas pressure in the anode region of the source, mm Hg	$5\cdot10^{-3}$
Group rate, Hz	2…10
Modulator arc pulse duration, μs	500
Magnetic field at the source, Oe	300…700
Modulator pulse duration of high voltage, μs	800

The elemental compositions of samples are as follows (%):

TiO_2-1 (ρ = 3.9 g/cm^3 = $8.865\cdot10^{22}$ atoms/cm^3): TiO_2-90.512, Na-5.633, Mg-0.005, Al-0.541, Si-0.717, P-0.136, S-0.169, Cl-0.127, Ca-0.079, V-0.750, Fe-0.121, Zn-0.745, Zr-0.043, Nb-0.105, Sb-0.318;

TiO_2-2 (ρ = 3.6 g/cm^3 = $7.895\cdot10^{22}$ atoms/cm^3): TiO_2-95.1, Si-2.325, S-0.222, Cl-0.262, Ca-0.067, V-0.895, Fe-0.936, Ni-0.016, Cu-0.055, Zr-0.007, Nb-0.010, Mo-0.009, Pb-0.013, Sn-0.023, I-0.065.

A thickness of samples was ~ 1 mm and a diameter was 15 mm. The helium ion beam was focused at a diameter of 10 mm. A temperature of samples during irradiation was ~ 60 °C.

2. EXPERIMENTAL RESULTS

A technique of the ceramic materials studies is as follows: after the certain irradiation dose, at 0.12 MeV energy, the microscopic and electrophysical studies of TiO_2-1 and TiO_2-2 samples were carried out.

From photos of the samples front and back sides made on the optical and electron microscopes, it follows that the surfaces are inhomogeneous, have a developed relief, which shows traces from the ion beam and craters, samples material splashing. Flecking formation is clearly visible on the samples both sides. Flecking fill factors are: k = 0.32 for the front side, k = 0.24 for the back side. It follows from the microscopic studies that with irradiation dose increasing the diffusion channels appear along the formed flecking perimeter, as well as directly in the flecking formation area. The flecking fill factor increases up to a dose of ~10^{17} ions/cm^2, after that it remains almost constant. The average value of the flecking depth on the samples front and back sides is ≈ 0.08 μm. The maximum depths also coincide and are ≈ 0.205 μm. Such equality of the geometric values can speak about coincidence of the physical mechanisms of the flecking formation on the samples front and back sides.

After TiO_2-1 and TiO_2-2 irradiating with helium ions, X-ray diffraction studies were performed on the samples front and back sides. Note the increase in titanium percentage content and decrease in oxygen content on the samples front and back sides. This change can only be explained by the dissociation of TiO_2 with the subsequent diffusion of oxygen to the sample surfaces and its partial output over the sample limits. In addition, there is the slight segregation of sample elements on its surface.

After the samples were irradiated with helium ions with a certain dose, the volume and surface electrical resistances of the samples front and back sides were measured. Figs. 1, 2 show the dependences of the change in the surface electrical resistances of the front and back sides of TiO_2-1 and TiO_2-2 samples on the irradiation dose.

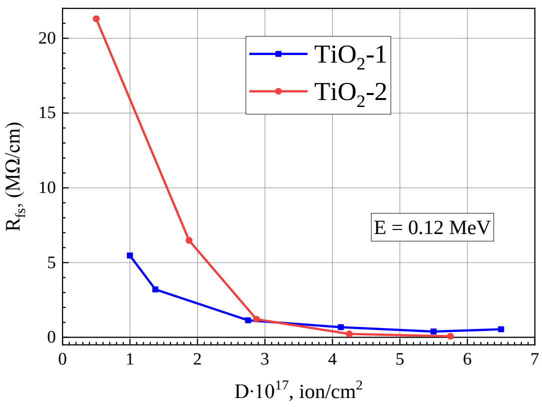

Fig. 1. Dependences of the surface electrical resistances of TiO_2-1 and TiO_2-2 samples (face sides) on the irradiation dose

Fig. 3 shows the dependences of the change in the volume electrical resistances of TiO_2-1 and TiO_2-2 samples on the irradiation dose. Fig. 4 shows the dependences of the change in the loss angle tangents for TiO_2-1 and TiO_2-2 samples on the irradiation dose.

Relative dielectric permittivity of samples was calculated: $\varepsilon = C \cdot d / (\varepsilon_0 S)$, where C is a capacitance; d is a sample thickness; S is a sample area; ε_0 is the absolute dielectric constant of vacuum (electrical constant), $\varepsilon_0 = 8.85 \cdot 10^{-12}$ F/m. Fig. 5 shows the dependences of the relative dielectric permittivities of samples on the irradiation dose.

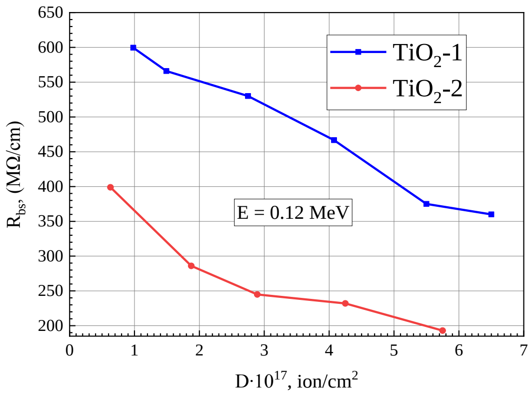

Fig. 2. Dependences of the surface electrical resistances of TiO_2-1 and TiO_2-2 samples (back sides) on the irradiation dose

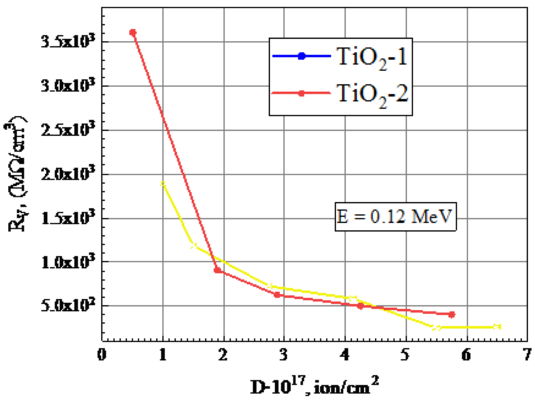

Fig. 3. Dependences of the volume electrical resistances of TiO_2-1 and TiO_2-2 samples on the irradiation dose

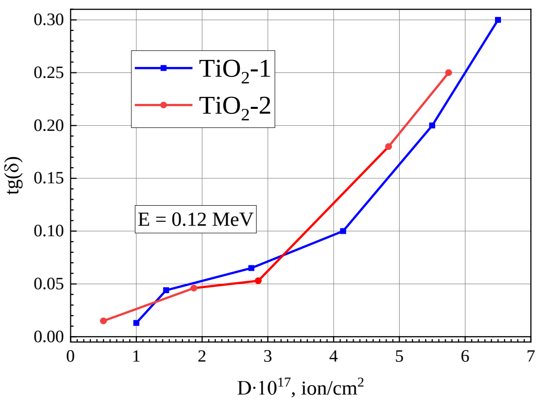

Fig. 4. Dependences of the loss angle tangents of TiO_2-1 and TiO_2-2 samples on the irradiation dose

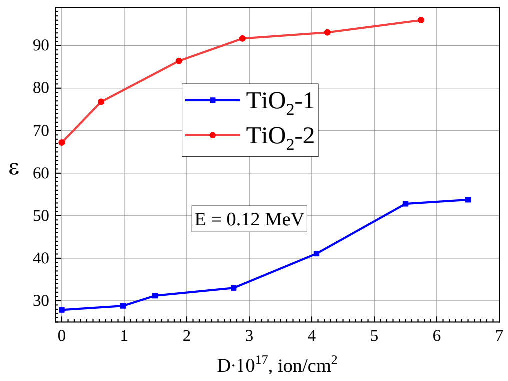

Fig. 5. Dependences of the relative dielectric permittivities of TiO_2-1 and TiO_2-2 samples on the irradiation dose

It follows from the above results that the decrease of the surface electrical resistances on the samples front sides occurs up to irradiation doses of ~ $5{\cdot}10^{17}$ ions/cm^2. On the samples back sides, the surface electrical resistance continues to decrease. The volume electrical resistance decreases to irradiation doses of ~ $(5…6){\cdot}10^{17}$ ions/cm^2.

The loss angle tangent and relative dielectric permittivity of the irradiated samples increase with the irradiation dose increasing. Such changes in the electrophysical characteristics can only occur due to TiO_2 dissociation and segregation of TiO_2-1 and TiO_2-2 elements over the samples volume.

3. CALCULATION CHARACTERISTICS

The primary processes occurring in the course of the irradiation, namely: the ionization, phonons and vacancies formation, segregation, sputtering, play an important role in the electrophysical characteristics change of the irradiated samples. The calculations were performed in the SRIM program [20] taking into account the displacement cascades.

3.1. SPUTTERING

When TiO_2-1 and TiO_2-2 samples are irradiated with 0.12 MeV helium ions energy, the surface changes occur as a result of the atoms sputtering of the samples structure and flecking formation [21]. These processes change the surface roughness. As the irradiation dose to the sample is dialed in, the hollows depth on the sample surface becomes greater and greater. The sputtering efficiency increases as each surface atom is bound to it with a small electrons number. After irradiation of TiO_2-1 and TiO_2-2 samples, the micrographs were taken, which showed that the front and back surfaces were heterogeneous, had a developed relief, and the hollows maximum depth was no more than 5 Å [18, 21]. When the sample surface relief change, the entry angle of helium ions into a sample also change, and the sputtering ratios of the sample elements change. When calculating of the sputtering ratios in the SRIM program, these facts were taken into account by changing of the ion entry angle into the irradiated samples and the hollows maximum depth.

Table 3 summarizes the total sputtering ratios and sputtering ratios of TiO_2-1 and TiO_2-2 main elements. It should be noted that the sputtering ratios were calculated at the uniform distribution of an entry angle 0…90° and at the hollows depth average of 2.5 Å.

Fig. 6 shows the dependences of the layer-by-layer variation of the total sputtering ratios along the depth of TiO_2-1 and TiO_2-2 samples under the irradiation by helium ions with 0.12 MeV energy at zero entry angle.

Table 3

Sputtering ratios ($k{\cdot}10^{-3}$, atom/ion) of TiO_2-1 and TiO_2-2 samples at helium ion energy of 0.12 MeV

Element	Entry angle 0°	Entry angle 0…90°	Entry angle 0…90° + roughness
TiO_2-1, ρ = 3.9 g/cm^3			
O	10.1	102.8	21.1
Ti	2.98	33.6	5.23
Na	4.66	44.5	9.16
Sum	17.9	180.9	35.5
TiO_2-2, ρ = 3.6 g/cm^3			
O	17.1	87.0	20.8
Ti	4.5	27.9	6.56
Si	0.36	2.2·10	0.57
Sum	22.45	117·10	28.4

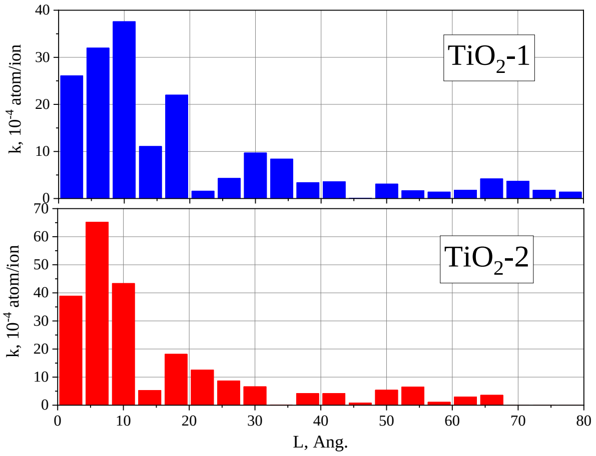

Fig. 6. Dependences of the total sputtering ratios on the depth of TiO_2-1 and TiO_2-2 sample, E = 0.12 MeV, at zero entry angle of helium ions

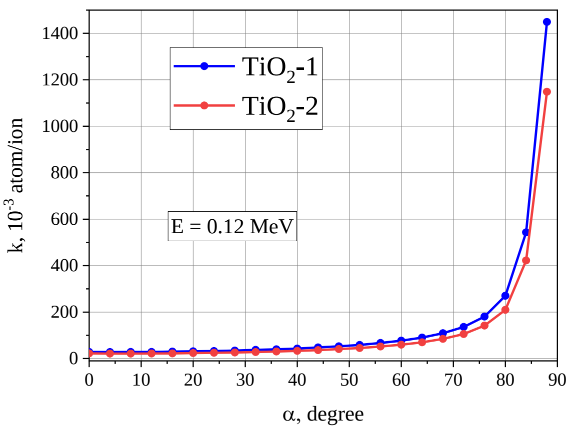

Fig. 7. Dependences of TiO_2-1 and TiO_2-2 sputtering ratios on the entry angle of helium ion beam without taking into account surface roughness, E = 0.12 MeV

It follows from these dependencies that calculations of sputtering ratios should not be performed for the sample depths greater than 80 Å.

Figs. 7 and 8 show the dependences of the total sputtering ratios of TiO_2-1 and TiO_2-2 samples on the entry angle of helium ion beam at 0.12 MeV energy.

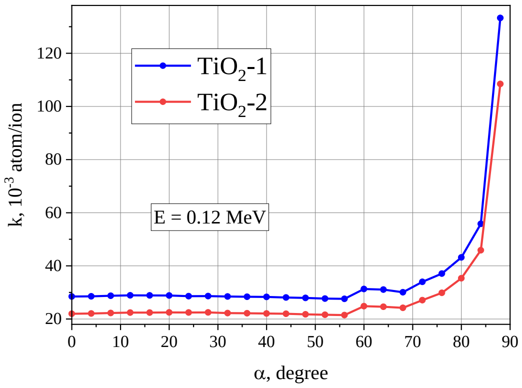

Fig. 8. Dependences of TiO_2-1 and TiO_2-2 sputtering ratios on the entry angle of helium ion beam taking into account the surface roughness, E = 0.12 MeV

As it follows from the graphs, taking into account the surface roughness of samples leads to a decrease in the sputtering ratios. Decreasing the initial sample density, the total sputtering ratio decrease. It should be noted that elements with a content of less than 5 % can be disregarded when calculating the total sputtering ratios. In our opinion, the true total sputtering ratios for TiO_2-1 and TiO_2-2 samples when irradiation by helium ions with 0.12 MeV energy are in the range of $1.8 \cdot 10^{-2}$ to $3 \cdot 10^{-2}$ atom/ion.

3.2. IONIZATION, PHONONS, AND VACANCIES FORMATION, SEGREGATION

The SRIM program was also used to calculate ionization profiles, phonons and vacancies formation, segregation in TiO_2-1 and TiO_2-2 samples. The calculations were carried out at zero entry angle of helium ions and at the entry angles 0...90° with an angle step of 2°, the total number of helium ions was $9 \cdot 10^6$. In Table 4 for TiO_2-1 and TiO_2-2 sample the energy losses going to the ionization, phonons formation and damage by helium ion beam and displacement cascades for irradiation energy E = 0.12 MeV are given. The absolute values of energies of these processes are given in the same Table.

As follows from Table 4, the beam energy most goes to the ionization (> 94 %). The main contribution to the ionization is made by helium ions. Phonons formation and damage is mainly due to displacement cascades. More than 5 times more energy is spent on phonons formation due to displacement cascades than due to helium ions. Phonons formation, at 0.12 MeV beam energy, consumes more than 17 times as much energy as a damage. Consequently, the phonons and ionization role in some radiation processes is determinative.

In Figs. 9, 10 the profiles of the ionization, phonons and vacancies formation, segregation in TiO_2-2 at 0.12 MeV helium beam energy, at zero entry angle and the entry angles uniform distribution of helium ions into the sample, respectively, are shown in the arbitrary units.

Table 4

TiO_2-1 and TiO_2-2 sample calculation characteristics

TiO_2-1, ρ = 3.9 g/cm^3, ion range maximum = 0.75 μm		
Loss of energy, %		
Ionization, He^+/cascade	Phonons, He^+/cascade	Damage, He^+/cascade
Zero entry angle		
93.85/1.07	0.76/4.04	0.08/0.20
Absolute energy values, keV/ion		
113.9	5.8	0.3
Entry angle 0...90°		
94.00/1.05	0.73/3.95	0.07/0.20
Absolute energy values, keV/ion		
114.06	5.62	0.32
TiO_2-2, ρ = 3.6 g/cm^3, ion range maximum = 0.85 μm		
Loss of energy, %		
Ionization, He^+/cascade	Phonons, He^+/cascade	Damage, He^+/cascade
Zero entry angle		
93.77/1.06	0.76/4.13	0.08/0.20
Absolute energy values, keV/ion		
113.8	5.9	0.3
Entry angle 0...90°		
93.93/1.04	0.74/4.02	0.08/0.19
Absolute energy values, keV/ion		
114.0	5.7	0.3

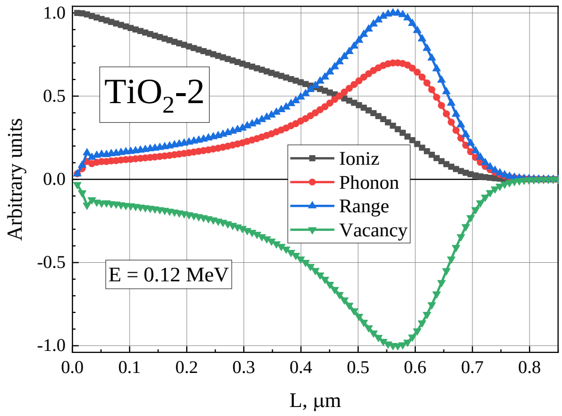

Fig. 9. Profiles of the ionization, phonons and vacancies formation, segregation in TiO_2-2 sample under helium ion irradiation at zero entry angle

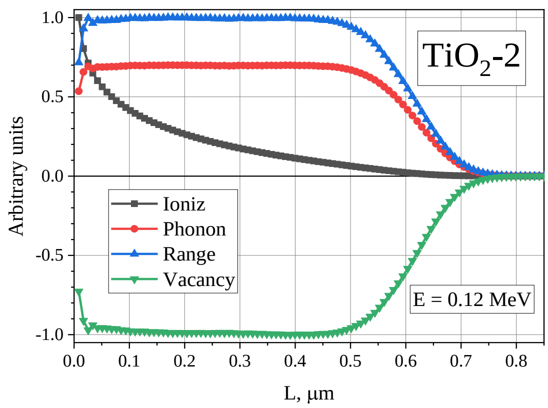

Fig. 10. Profiles of the ionization, phonons and vacancies formation, segregation in TiO_2-2 sample under helium ion irradiation at the entry angles 0...90°

For TiO_2-1 similar distributions were obtained considering the higher density (3.9 g/cm^3) and the different elemental composition (Section 1).

It follows from the obtained distributions that in TiO_2-1 and TiO_2-2 irradiated samples the segregation of the material atoms along helium ions range take place, which mainly determine the changes in the thermophysical and electrophysical characteristics of the irradiated samples. Table 5 shows the main element ratios of TiO_2-1 and TiO_2-2 redistributed atoms to helium atoms.

Table 5

Main element ratios of TiO_2-1 and TiO_2-2 redistributed atoms to helium atoms

TiO_2-1						
	O/He	Ti/He	Na/He	Mg/He	Al/He	Si/He
A	55.68	37.75	19.75	0.002	0.20	0.46
B	55.59	36.70	20.44	0.0018	0.20	0.47
	P/He	S/He	Cl/He	Ca/He	V/He	Fe/He
A	0.05	0.064	0.048	0.031	0.28	0.046
B	0.052	0.066	0.049	0.031	0.28	0.046
	Zn/He	Zr/He	Nb/He	Sb/He	–	
A	0.28	0.015	0.037	0.31		
B	0.28	0.015	0.037	0.31		
TiO_2-2						
	O/He	Ti/He	Si/He	S/He	Cl/He	Ca/He
A	64.14	42.71	6.12	0.35	0.41	0.11
B	69.5	43.7	6.3	0.36	0.42	0.11
	V/He	Fe/He	Ni/He	Cu/He	Zr/He	Nb/He
A	1.37	1.46	0.025	0.085	0.01	0.026
B	1.4	1.5	0.03	0.09	0.01	0.03
	Mo/He	Pb/He	Sn/He	I/He	–	
A	0.032	0.016	0.032	0.088		
B	0.03	0.02	0.03	0.09		
A – entry angle 0°, B – entry angle 0...90°						

From these data the segregation atoms number is calculated as a function of the irradiation dose.

3.3. DAMAGE

Vacancies formation and the number of displacements per ion in TiO_2-1 and TiO_2-2 samples play a major role in the damage calculations (dpa is the number of displacements per atom). This expression was used to calculate dpa [18]:

$$dpa = \frac{D_{ion} \cdot dpi}{N_A \rho_0 SL} \cdot M,$$

where D_{ion} is the irradiation dose (ion/cm^2, experimental parameter); dpi is the number of displacements per ion (from the SRIM calculations); N_A is Avogadro number; ρ_0 is the measured sample density; S = 1 cm^2 is the sample unit area; L is the maximum ion range in the sample; $M = (1/100)\sum_i \mu_i n_i$ is the sample molar mass; μ_i is the molecular mass of the sample i-th element; n_i is the percentage content of the sample i-th element. Table 6 summarizes the main characteristics of TiO_2-1 and TiO_2-2 samples that were used for the calculations.

Table 6

Main characteristics of irradiated samples

Sample	Vacancy, vac./ion A/B	dpi, dis./ion A/B	dpa, dis./atom A/B
TiO_2-1	112/107	114/109	52.1/49.4
TiO_2-2	114/108	116/111	50.3/48.1
A – entry angle 0°, B – entry angle 0...90°			

Damages (dpa) were calculated for the irradiation doses of $1 \cdot 10^{18}$ ions/cm^2. The dpa profiles in TiO_2-1 and TiO_2-2 samples are shown in Figs. 11 and 12, at zero entry angle of helium ions and at the entry angles of 0...90°.

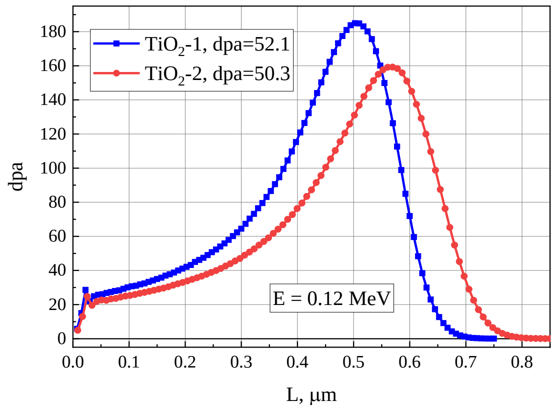

Fig. 11. Damage profiles in TiO_2-1 and TiO_2-2 samples under helium ion irradiation at zero entry angle

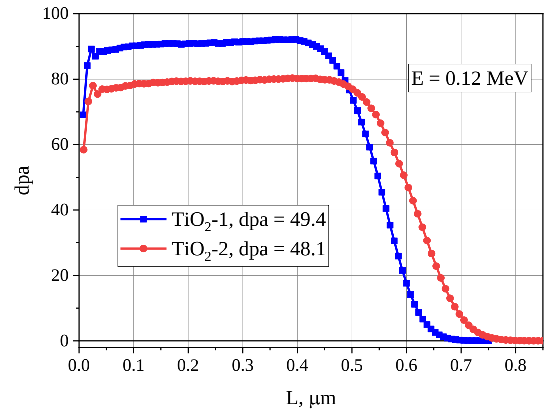

Fig. 12. Damage profiles in TiO_2-1 and TiO_2-2 samples under helium ion irradiation at entry angles of 0...90°

It follows from calculations that taking into account the entry angles of helium ions into the sample leads to the damage profile broadening toward smaller range values and to an overall decrease in the dpa value.

4. ANALYSIS AND DISCUSSION OF RESULTS

When measuring the electrophysical characteristics of TiO_2-1 and TiO_2-2 irradiated samples (helium ion energy was 0.12 MeV), with the irradiation dose increasing, it was found: decrease of the surface electrical resistances on the samples front and back sides (see Figs. 1, 2); reduction of the volume electrical resistances (see Fig. 3); increase in the loss angle tangents and relative dielectric permittivities (see Figs. 4, 5). The surface electrical resistivity decrease on the sample front sides occurs up to doses of ~ 5·10^17 ion/cm^2. On the sample back sides, the surface electrical resistivity decrease is observed within of the dialed doses. The volume electrical resistivity decrease occurs up to the irradiation doses of ~ (5…6)·10^17 ions/cm^2. The increase in the loss angle tangents and relative dielectric constants of the samples occurs within of the dialed irradiation doses.

The obtained experimental results can be explained by the complex influence of the primary processes (Section 3) on the structure change of TiO_2-1 and TiO_2-2 irradiated samples. Sputtering of the structure atoms (see Section 3.1) affects only the sample face at the expense of the surface relief changing. This leads to the primary processes changes in helium ion area range, and hence in secondary processes changes such as the diffusion, re-segregation, phonons re-generation, etc.

Using the model of the elastic wave excitation and their propagation through the volume of samples [12, 13, 21], we can explain the changes in the electrophysical characteristics of TiO_2-1 and TiO_2-2 irradiated samples. Phonons formation (see Section 3.2) occurs in the regions of the ionization, segregation and vacancies formation. The propagation of longitudinal waves occurs both in the direction of the sample front surface and in the direction of the back surface. The main contribution to phonons formation is made by the displacement cascades (see Table 4). In the region where the helium ions are traveling, there is a high-frequency shock wave formed by the displacement atoms and a low-frequency shock wave formed by helium ions. Using the calculated results (see Section 3), the averaged dependences of phonons formation due to the displacement cascades and helium ions are obtained. Fig. 13 shows the phonons formation profiles along the path length of helium ions in TiO_2-1 and TiO_2-2 samples.

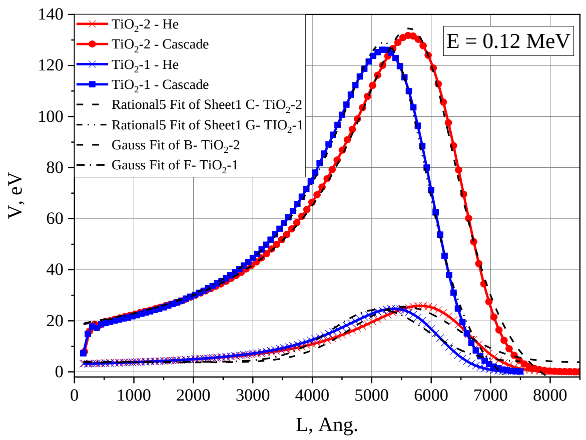

Fig. 13. Phonons formation profiles in TiO_2-1 and TiO_2-2 samples under the action of helium ions and displacement cascades

The dependences obtained for TiO_2-1 and TiO_2-2 can be described by the following extrapolation expressions.

Phonons formation by the displacement cascades:

$$V_{a.h.f.} = \frac{a + b \cdot L}{1 + c \cdot L + d \cdot L^2}. \quad (1)$$

Phonons formation by helium ions:

$$V_{He}(L) = V_0 + \left(\frac{A}{\omega\sqrt{\pi/2}}\right) \cdot \exp\left(-2 \cdot \left(\frac{L - L_C}{\omega}\right)^2\right). \quad (2)$$

Table 7 shows the values of constants for expressions (1) and (2).

Table 7

Values of constants for expressions (1) and (2)

Sample	a	b	c	d
TiO_2-1	18.1	-0.0025	$-3.5 \cdot 10^{-4}$	$3.18 \cdot 10^{-8}$
TiO_2-2	18.5	-0.0024	$-3.2 \cdot 10^{-4}$	$2.72 \cdot 10^{-8}$
V_0		A	ω	L_C
TiO_2-1	3.90	41086.4	1593.9	5116.9
TiO_2-2	3.70	48240.8	1764.7	5537.8

Fig. 14 shows the fragments of the high-frequency waves formation in TiO_2-1 and TiO_2-2 samples for account of the displacement cascades.

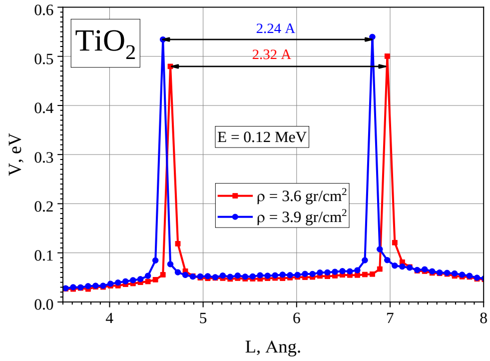

Fig. 14. Fragments of the high-frequency waves formation for account of the displacement cascades

From this figure, it can be seen that the displacement cascades form the high-frequency shock waves. Expression (1) describes the amplitude (envelope curve) of these waves. Table 6 shows that there are ~ 109…116 displacements per helium ion with the following formation of the high-frequency shock waves with amplitudes up to 130 eV. The profile of the high-frequency shock wave can be described by the following expression:

$$V_{h.f.}(L) = V_{a.h.f.} + \frac{A_0}{\omega\sqrt{\pi/2}} \cdot \exp\left(-2\frac{L - L_C}{\omega^2}\right), \quad (3)$$

where $V_{a.h.f.}$ is obtained from expression (1), ω = 0.039; A_0 = 0.046; L_C is the distance of the high-frequency wave formation from the sample surface.

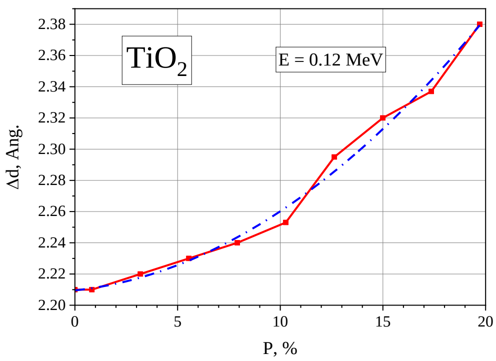

Fig. 15. Dependences of the peak spacing on a porosity of TiO_2-based samples

As can be seen from Fig. 14, the high-frequency wave maxima take discrete values with a step depending on the sample initial density. Fig. 15 shows the dependences of the peak spacing on a porosity of TiO_2-based samples.

This dependence can be described by the expression:

$$\Delta d = a_0 + a_1 P + a_2 P^2, \qquad (4)$$

where P is a porosity in %; a_0 = 2,21 Å is the distance between peaks at zero porosity (minimum parameter of the TiO_2 elementary lattice); a_1 = 0.0014; a_2= $3.7\cdot10^{-4}$.

The process of the propagation of the generated phonon oscillations can be described by a wave equation with the initial conditions for the formation of the high-frequency and low-frequency acoustic waves, taking into account the changes in the sample density $\rho(h,t)$ along its thickness. The sample density is calculated for the different irradiation doses taking into account the segregation and vacancies formation (Chapter 3). The initial conditions are written:

$$V\left(L, t=0\right) = V_{He}(L) + \sum_{i=1}^{i} V_{h.f.}(L), \qquad (5)$$

where $V_{He}(L)$ is the low-frequency mode (2); $V_{h.f.}(L)$ is the high-frequency mode (3); i is the number of the high-frequency excitation modes in a sample per one helium ion, depends on the sample initial porosity. The L_C value in expression (3) is determined in a random way using expression (4).

The processes of the ionization and formation of low-frequency and shock waves occur cyclically throughout the sample volume. The energy transfer by acoustic waves is sufficient to dissociate of TiO_2 (the binding energy of TiO_2 is about of 10 eV) and efforts formation throughout the volume of samples.

The flecking formation, titanium percentage content increase and oxygen decrease on the front and back sides of TiO_2 irradiated samples were experimentally found in [18]. These processes are also described by the wave equation for the thermoelastic and deformation volume forces propagation due to the acoustic waves formation. The diffusion of oxygen and helium plays a significant role in the flecking formation, which occurs mainly through the channels formed along the flecking perimeter, as well as directly in an area of its formation.

CONCLUSIONS

1. The long-range effect has been confirmed on the basis of the experimental results, i. e. the change in the electrophysical characteristics of TiO_2-1 and TiO_2-2 samples with the increasing irradiation dose by helium ions with 0.12 MeV energy.

2. The primary processes during irradiation of TiO_2-based samples, namely, the ionization, phonons and vacancies formation, segregation, damage and sputtering have been calculated.

3. The analysis of experimental results and calculated data showed that the processes of the formation and propagation of the low-frequency and high-frequency shock waves play a determining role in the changing the electrophysical characteristics of the irradiated samples. Analytical expressions for the initial conditions of the wave equation are obtained.

The model based on the primary radiation processes of the excitation and propagation of the elastic waves most physically correctly describes the experimental results obtained by the irradiation of TiO_2-1 and TiO_2-2 samples at the linear helium ions accelerator with 0.12 MeV energy.

REFERENCES

1. D.I. Tetelbaum, E.V. Kuril'chik, Ya.A. Mendeleva. Long-range interaction effect at the low-intensity irradiation of solids // *Surface*. 2009, № 3, p. 1-11.
2. N.P. Morozov, D.I. Tetelbaum. Deep penetration of radiating defects from the ion-implanted layer in semiconductor volume // *Physics and technics of semiconductors*. 1983, v. 17, issue 5, p. 838-842.
3. Yu.P. Sharkeev, E.V. Kozlov, A.N. Didenko, et al. The mechanisms of the long-range effect in metals and alloys by ion implantation // *Surface and Coating Technology*. 1996, v. 83, p. 15-21.
4. C.A. Krivelevich. Switching waves and long-range interaction effects // *The bulletin of the Nizhniy Nov-gorod university. Solid physics.* 1998, issue 2, p. 71-78.
5. D.I. Tetelbaum, E.V. Kuril'chik, N.D. Latisheva. Long-range effect at low-dose ion and electron irradiation of metals // *Nucl. Instrum. and Meth. in Phys. Res.* 1997, B127/128, p. 153-156.
6. Yu.V. Martynenko, P.G. Moskovin. Long-range effect and energy transfer in solids under ion bombardment // *Letters to the Journal of Technical Physics*. 1996, v. 22, issue 17, p. 54-58.
7. Yu.P. Sharkeev, A.N. Didenko, E.V. Kozlov. High dislocation density structures and hardening produced by high fluency pulsed into beam implantation // *Surface and Coating Technology*. 1994, v. 65, p. 112-120.
8. D.I. Tetelbaum, A.Yu. Azov, E.V. Kuril'chik, et al. The long-range influence of the ion and proton irradiation on the mechanical properties and on the composition of the permaloy-79 // *Vacuum*. 2003, v. 70, № 2-3, p. 169-173.
9. N.P. Morozov, V.D. Skupov, D.I. Tetelbaum. In silicon defect formation at ion bombardment outside of ions range area // *Physics and technics of semiconductors.* 1985, v. 19, issue 3, p. 464-468.
10. D.I. Tetelbaum, V.Ya. Bayankin. Long-range interaction effects // *Priroda*. 2005, № 4, p. 9-17.
11. N.P. Aparina, M.I. Guseva, B.N. Kolbasov, et al. Some aspects of the long-range interaction effect // *Problems of Atomic Science and Technology*. 2007, № 3, p. 18-27.
12. F. Mirzoev. Distribution of nonlinear longitudinal waves in solids taking into account fields interaction of defects deformation and concentration // *Journal of Technical Physics.* 2002, v. 72, issue 10, p. 53-57.
13. A.I. Kalinichenko, V.E. Strel'nitskij. Elastic waves generated at ion implantation and their influence on processes in irradiated matter // *Problems of Atomic Science and Technology. Series "Physics of Radiation*

Effect and Radiation Material Science". 2005, № 5, p. 159-163.

14. V.O. Bomko, O.F. Dyachenko, O.M. Yegorov, et al. Development of investigations on the MILAC heavy ion linear accelerator // *Proc. of the LINAC08, Vancouver, Victoria, Canada.* 2008, p. 187-189.

15. S.N. Dubniuk, R.A. Anokhin, A.F. Dyachenko, et al. Radiation complex on the basis of helium ions linac // *Problems of Atomic Science and Technology. Series "Plasma Electronics and New Methods of Acceleration".* 2018, № 4, p. 46-51.

16. A.F. Dyachenko, R.A. Anokhin, S.N. Dubniuk, et al. The bunch formation and transport system to the target of the helium ions linac // *Problems of Atomic Science and Technology. Series "Plasma Electronics and New Methods of Acceleration".* 2018, № 4, p. 52-55.

17. V.I. Butenko, S.N. Dubniuk, A.F. Dyachenko, et al. Tribological characteristics of steel ceramics irradiated by helium ions pair // *Problems of Atomic Science and Technology. Series "Physics of Radiation Effect and Radiation Material Science".* 2021, № 5, p. 44-50.

18. V.I. Butenko, A. Cenian, O.F. Dyachenko, et al. TiO_2-2 radiating damages as a result of the irradiation helium ions with energies of 0.12 and 4 MeV on the linear accelerator // *Problems of Atomic Science and Technology. Series "Plasma Electronics and New Methods of Acceleration".* 2023, № 4, p. 96-104.

19. R.A. Anokhin, B.V. Zaitsev, K.V. Pavlii, et al. Experimental complex for investigation of construction materials on the helium ions linear accelerator // *Problems of Atomic Science and Technology. Series "Nuclear Physics Investigations".* 2017, № 6, p. 167-171.

20. http://www.srim.org.

21. A.I. Kalinichenko, S.S. Perepelkin, V.E. Strel'nitskij. On shaping of craters at ion bombardment // *Problems of Atomic Science and Technology. Series "Physics of Radiation Effect and Radiation Material Science".* 2013, № 2(84), p. 167-171.

Article received 25.09.2024

ЕЛЕКТРОФІЗИЧНІ ХАРАКТЕРИСТИКИ ЗРАЗКІВ TiO_2, ОПРОМІНЕНИХ ІОНАМИ ГЕЛІЮ З ЕНЕРГІЄЮ 0,12 МеВ

К.В. Павлій, С.М. Дубнюк, О.Ф. Дьяченко, О.В. Мануйленко, Б.В. Зайцев

Наведено основні параметри опромінення зразків на лінійному прискорювачі іонів гелію, а також характеристики опроміненого TiO_2. Експериментально показано, що зі збільшенням дози опромінення (енергія іонів гелію 0,12 МеВ) зменшуються об'ємні електроопори і поверхневі електроопори на лицьовій і тильній сторонах зразків, збільшуються тангенси кута втрат і відносні діелектричні проникності. Розраховано первинні процеси: напилення, іонізації, утворення фононів і вакансій, сегрегації, пошкоджуваності. Аналіз експериментальних і розрахункових даних засвідчив, що модель, заснована на процесах збудження й поширення пружних хвиль у концепції ефекту далекодії, найбільш фізично коректно описує змінення електрофізичних характеристик опромінених зразків.